

**European Commission Center of Excellence
Inter-Disciplinary Research and Applications
based on Nuclear and Atomic Physics**

*From: HORIA HULUBEI NATIONAL INSTITUTE OF PHYSICS AND NUCLEAR
ENGINEERING (IFIN -HH)*

Str. Atomistilor 407, P.O. Box MG-6

RO-76900 BUCHAREST-Măgurele, ROMANIA

Tel: 0040 1 404 23 00, Fax: 0040 1 457 4440

E-mail: cex@ifin.nipne.ro, http://www.nipne.ro/Cenex/cex_eur.htm

Report WP4 IDRANAP 51-03 / 2003

**Development of analysis methodology using
Particle Induced X-ray Emission (PIXE) as a
complementary method to determine some heavy metals**

Constantin Ciortea, Ion Piticu, Dana Elena Dumitriu, Alexandru Enulescu,
Daniela Fluerasu, Marius Marin Gugiu, Aimee Theodora Radu,
Lucretia C. Dinescu, Magdalena Haralambie and Ana Stoichioiu

*Horia Hulubei National Institute of Physics and Nuclear Engineering,
Magurele, P.O. Box MG-6, RO-76900 Bucharest, Romania*

* Work supported in part by the Center of Excellence IDRANAP under ICA1-CT-2000-70023 Contract with European Commission, and by the Ministry of Education and Research

Abstract

The proton induced X-ray emission (PIXE) method is well suited for quick quantitative analysis of thick targets like metal alloys or sediment / soil pellets, reported here.

In the present metal alloys (medieval Romanian silver coins, XIVth century) analysis, no measurements with standards were necessary. The elemental composition is deduced directly from the measured relative X-ray intensities, using known X-ray production cross sections and correcting for proton energy loss, X-ray attenuation in the sample and detector efficiency; also a correction scheme for secondary X-ray fluorescence was included. Apart from Ag, other analysed elements in the coins were Cu, Pb, Au, Fe and Pt. The analysis procedure for metal alloys was checked by analysis of thick samples of known composition.

For complex (sediment / soil) samples, an experimental calibration based on standards was applied. Using beam current integration as normalisation procedure, an experimental thick target factor, to convert thin sample X-ray intensities in thick target element concentrations, was determined.

PACS: 29.30.Kv; 82.80.Jp; 78.70.En; 89.60.-k

Keywords: Metal alloy and sediment / soil analysis; thick target PIXE.

1. Introduction

A PIXE programme has been introduced about ten years ago in Tandem Laboratory of NIPNE, Bucharest, for routine analysis of samples as different as ancient metal alloys or human serum and tissues. Here we report the present effort for development of the thick target PIXE method, in particular directed to the applications for metal alloys and sediment/soil analysis.

PIXE as a fast, non-destructive, multielement and sensitive analytical tool is based on the spectral analysis of characteristic X-rays emitted from matter under bombardment by energetic charged particles, namely protons. It is an alternative to other excitation modes, like X-ray fluorescence (XRF) with incident photons (XRF using synchrotron radiation gives performances

comparable with PIXE). The advantage of PIXE is that small quantities can be effectively analysed, being ideal for analysis of e.g. some types of biological samples, aerosols etc.

The use of thick targets (specimens) is important for some types of samples or in ion microprobe analysis. The advantage of thick specimens is that they are simpler to prepare. For quantification of thick target PIXE analysis, the absolute yield method could be used with reasonable accuracy [1]. In this method, the yield of characteristic X-rays are converted to elemental concentrations using a data base of X-ray production cross sections, X-ray attenuation coefficients and ion stopping powers, together with measurements of the absolute efficiency of the detector. In metal alloys analysis, like silver alloys reported here, the elemental composition could be deduced directly from the measured relative X-ray intensities by using known X-ray production cross sections and correcting for proton energy loss, X-ray attenuation in the sample and detector efficiency, and by carrying out some numerical calculations [2-4].

The applications of this absolute yield method to multielement, complex samples, like sediment/soil, implies that the matrix composition (inclusive the light element fraction) has to be known. Instead, by using a standard sample having a similar matrix composition as the unknown one, and a properly normalisation procedure, an experimental thick target factor, which convert thin sample X-ray intensities in thick element concentrations could be determined [5].

In the present report, the absolute yield method for analysis of silver alloys (medieval Moldavian coins, XIVth century), without standard measurement, and for complex (sediment/soil) samples, an experimental calibration based on standards and beam current integration was applied.

2. Experiment

In the PIXE method, fluorescence X-rays are emitted in consequence of inner-shell ionisation produced by energetic protons (or other charged particles) impinging onto the sample. A schematic drawing of the experimental arrangement is presented in Fig. 1. The Van de Graaff tandem accelerator of NIPNE, Bucharest, provides the 3 MeV proton beam. The samples, of metal alloys (medieval Moldavian coins) and sediment/soil (pressed pellets of 1-2 mm thickness and 10-12 mm diameter), were measured in vacuum. A collimated beam (2.5 mm diameter) bombarded the target oriented at an angle of 45° with respect to the beam direction. The whole scattering chamber, electrically isolated to the beam line, served as a Faraday cup. The beam

current entering the scattering chamber was maintained at several nA. The samples were irradiated for a collected charge, measured by using an ORTEC model 439 current digitizer, of typically 10 μC . The energy dispersive analysis of the X-ray spectrum is performed by a semiconductor (hyper-pure Ge) detector located at 90° relative the beam direction. In the case of metal alloy measurements, a 40 μm Aluminium foil in front of the detector was used in order to attenuate the high-intensity, low-energy X-rays or bremsstrahlung.

The signals from the detector preamplifier were processed with a Tennelec spectroscopic amplifier model TC244, enabling pile-up rejection, and then fed into a Canberra ADC and mixer-router model 1520 . Data manipulation and storage were performed with a Canberra S100 counting system, based on an IBM personal computer. The X-ray spectra were analysed using the code LEONE, which models the X-ray peaks with Gaussian functions and subtracts a polynomial background (of degree 1 - 3). The peak area derived from the fitting routine, corrected for X-ray attenuation and detector efficiency, was then used to determine the elemental concentrations.

3. Metal alloy X-ray yield calculation

The sample is assumed to be homogeneous and flat. The geometry is shown in Fig. 2.

The proton beam is bombarding the target at an angle α with the normal to target surface (45° in our experiment). The X-ray detector is positioned at 90° to the proton beam, subtending a small solid angle. The primary X-ray yield produced in a volume element of thickness ds at the depth s behind the target surface, corresponding to the element k present with a mass concentration c_k , due to a number Φ of impinging protons, is well described by the following integral over the target thickness:

$$\Gamma_{X,k}^{(prim)} = \Phi \frac{c_k N_A}{A_k} \omega_k \frac{\Gamma_k}{\Gamma} (\varepsilon f)_k \int ds \sigma_k(s) e^{-\mu_k s / \tan \alpha} \quad (1)$$

which takes into account the decreasing energy of the projectile entering the thick sample and the attenuation of the X-rays leaving the sample in the direction of the detector. In this relation, A_k is the atomic mass of the considered element, N_A - the Avogadro number; σ_k denotes the

ionisation cross section, which due to energy loss is variable with the depth s ; ω_k is the fluorescent yield and Γ_k/Γ_X - the fraction of the total X-ray emission of the analysed line (usually $K\alpha$ or $L\alpha$ X-rays); by μ_k - the absorption coefficients of primary X-rays and by $(\varepsilon f)_k$ - the detector efficiency and attenuation in windows and the Aluminium foil were denoted.

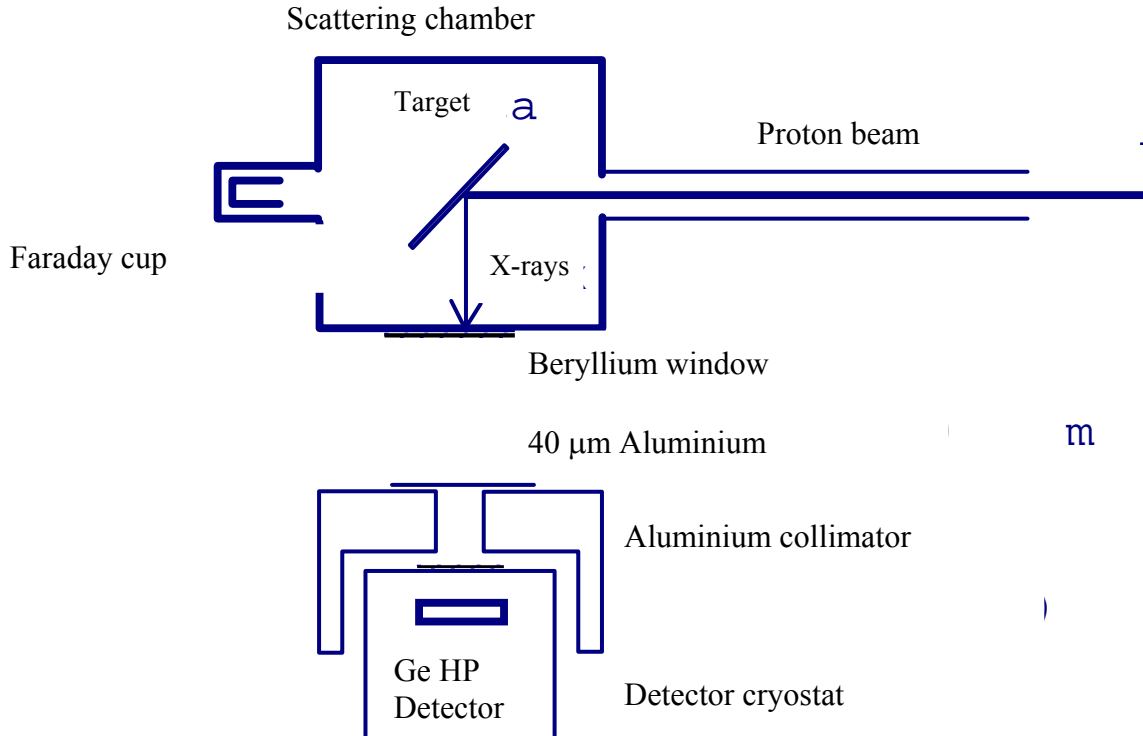


Figure 1. Schematic drawing of the experimental arrangement.

Only those primary X-ray lines j of the element i which have the energy larger than the K or L absorption edges of the element k can give rise to secondary X-rays. Let the absorption be within the volume element dV , with the spherical coordinates (r, θ) with respect to ds (we assumed spherical symmetry around the z axis). Taking into account the attenuation of the primary X-rays along the path r and the attenuation of the secondary X-rays along the path in the target

$\ell_k = s / \tan\alpha + r \cos\theta / \sin\alpha$ (see the two possible positions with respect to detector in Fig. 2, corresponding to $\theta \leq 90^\circ$ and $\theta \geq 90^\circ$), and summing over all primary X-rays, we obtain for the secondary X-ray yield the expression :

$$I_{X,k}^{(sec)} = \frac{1}{2} \Phi \frac{c_k N A}{A_k} \omega_k \frac{\Gamma_k}{\Gamma} (\varepsilon f)_k \sum_i \frac{c_i N A}{A_i} \omega_i \frac{\Gamma_j^i}{\Gamma_X^i} \sigma_{k(j)}^{(ph)} \int ds dr \sin \theta d\theta \sigma_j(s) e^{-\mu_j^r} e^{-\mu_k^l} \quad (2)$$

where $\sigma_{k(j)}^{(ph)}$ are the photoelectric cross sections for the absorption of the X-ray lines j leading to the secondary X-ray lines k . The integrals over r and θ could be effectuated analytically using the exponential integral $Ei(x)$ and were numerically evaluated by using series representations [6].

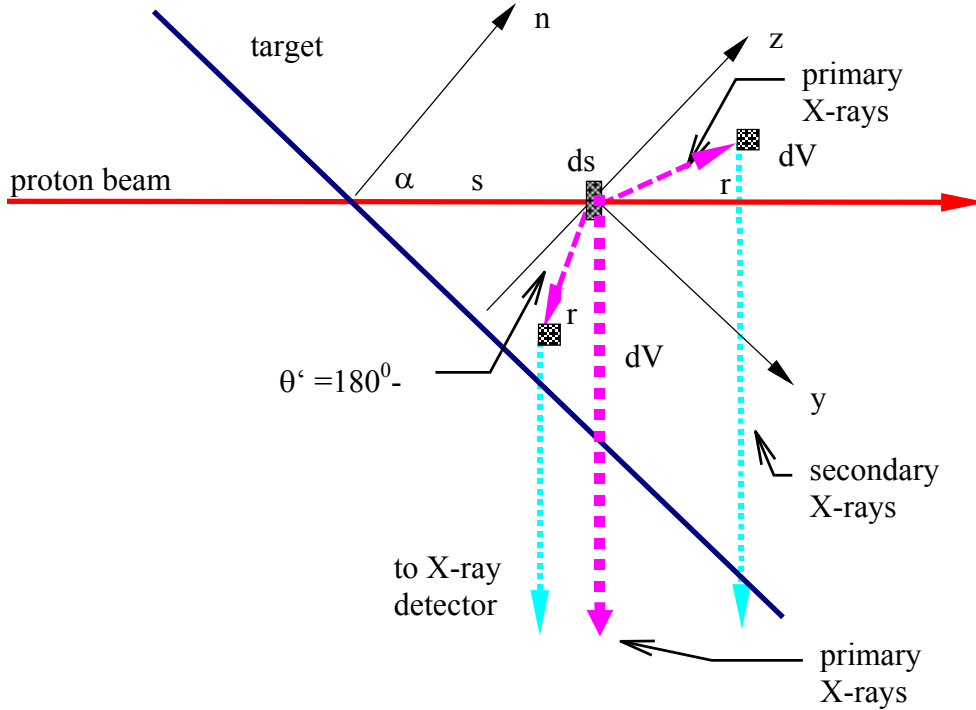


Figure 2. Schematic of the geometry of the experiment. y and z denote the coordinate axes (z normal to the target surface) having the origin in the volume element of thickness ds at depth s , where primary X-rays are produced. The primary X-rays reach the volume element dV , where they give rise to secondary X-rays (two possible positions are represented in the figure). The X-rays are detected at sufficiently small solid angle such that they are moving in the same direction, perpendicular to the beam direction.

The contribution of the secondary fluorescence is usually a correction to the primary fluorescence, given by the following ratio:

$$\frac{I_{X,k}^{(sec)}}{I_{X,k}^{(prim)}} = \frac{\sin \alpha}{2\mu_k} \frac{\sum_{i,j} c_i \omega_i \frac{\Gamma_j^i}{\Gamma_X^i} \sigma_{k(i)}^{(ph)} \left[\ln \left| \frac{\mu_j + \mu_k / \sin \alpha}{\mu_j - \mu_k / \sin \alpha} \right| S_{ik}^{(1)} + S_{ijk}^{(2)} \right]}{S_k^{(0)}} \quad (3)$$

where we noted:

$$S_k^{(0)} = \int ds \sigma_k(s) e^{-\mu_k s / \tan \alpha}, \quad (4)$$

$$S_{ik}^{(1)} = \int ds \sigma_i(s) e^{-\mu_k s / \tan \alpha}, \quad (5)$$

$$S_{ijk}^{(2)} = \int ds \sigma_i(s) \left\{ e^{-\mu_k s / \tan \alpha} Ei \left[s (\mu_k / \tan \alpha - \mu_j \cos \alpha) \right] - Ei \left(-s \mu_j \cos \alpha \right) \right\}. \quad (6)$$

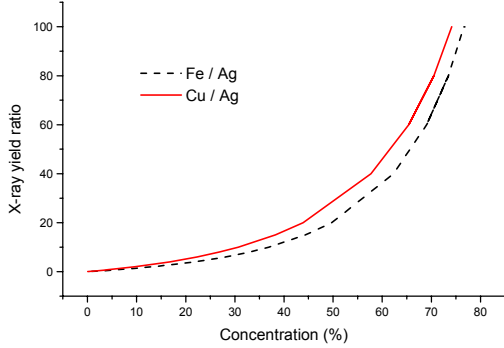


Figure 3. Results of the calculations for the binary alloys *Fe-Ag* and *Cu-Ag*. The X-ray yield ratios are represented in function of the Fe and Cu concentrations, respectively. The major X-rays in the spectra ($K\alpha$ for Fe and Ag and $L\alpha$ for Au) have been taken into account. The experimental conditions for detector efficiency and X-ray attenuation have been included.

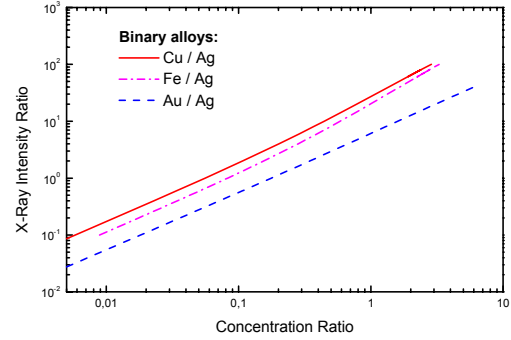


Figure 4. X-ray yield ratios in function of concentration ratios calculated for the binary alloys of *Cu-Ag*, *Fe-Ag* and *Au-Ag*. The notations are given in the figure. The major X-rays in the spectra ($K\alpha$ for Fe, Cu and Ag and $L\alpha$ for Au) have been taken into account. The experimental conditions for detector efficiency and X-ray attenuation have been included.

The integrals (4-6) have been calculated numerically with a computer code. The proton energy loss has been evaluated by using the semiempirical relations of Andersen and Ziegler [7], while the photoeffect and total attenuation coefficients from the compilation of Veigele [8] were taken. Tabulated ECPSSR ionisation cross sections [9], fluorescence yields [10] and partial radiative widths [11] were used.

4. Results

4.1. Metal alloys

We calculated X-ray fluorescence yields for some binary systems, see the Figs. 3 and 4. The X-ray yield ratios are presented in function of the concentration of one component of the alloy (Fig. 3) or the concentration ratio (Fig. 4). Relative enhancement due to secondary fluorescence (Fig.

5) attains its maximum value when the excited element is present as a trace. The enhancement effect is not important in the binary alloys comprising Ag; but it is significant e.g. in the Fe-Cu alloy.

The present analytical procedure has been tested by measuring some Cu-Ag alloys of known composition. A good agreement between the measured concentrations and the known ones was obtained, as is shown in Fig. 6. In Table 1 some results obtained by analysing Moldavian coins from XIVth century (National History Museum, Bucharest) are given.

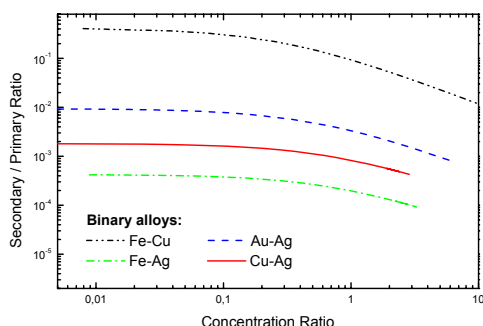


Figure 5. The secondary fluorescence contribution to the X-ray yields calculated for the binary alloys Fe-Cu, Au-Ag, Cu-Ag and Fe-Ag. The notations are given in the figure. The major X-rays in the spectra ($K\alpha$ for Fe, Cu and Ag and $L\alpha$ for Au) have been taken into account. Our experimental conditions for detector efficiency and X-ray attenuation have been included.

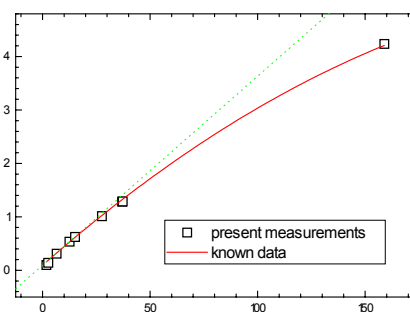


Figure 6. Comparison of the results of the present measurements (\square) with the known concentrations of standard Cu-Ag binary alloys (—). As can be seen, the ratios of X-ray yields and concentrations are not strictly proportional (the dotted line).

4.2. Sediment / soil samples

The concentrations of the sediment/soil samples have been determined by comparing to the standard sediment sample IAEA SL-1. The determined thick target factor (for the ratio element/Fe) is given in Fig. 7. Results obtained by using the normalisation to the beam current integrated charge, in the case of a sediment core collected from the lake Nebunu in Danube delta, are presented in Fig. 8.

Table 1. Element composition of some Moldavian coins (XIVth century) determined by TTPIXE method. The weight concentrations (%) are given.

<i>Elem./ coin no.</i>	<i>Fe</i>	<i>Cu</i>	<i>Ag</i>	<i>Au</i>	<i>Pb</i>	<i>Pt</i>	<i>Sn</i>
1	0,55	59,3	39,4	0,021	0,49	-	-
2	0,85	63,8	34,0	0,039	0,89	-	-
3	0,77	61,8	36,1	0,064	0,96	-	-
4	0,77	67,2	31,4	0,061	0,20	-	-
5	0,68	59,6	39,0	0,038	0,38	-	-
6	0,62	71,2	27,6	0,21	0,19	-	-
7	0,63	49,6	48,5	0,18	0,84	-	-
8	0,82	72,1	26,4	0,068	0,36	-	-
9	0,46	87,4	11,3	0,014	0,50	-	-
10	0,85	76,3	22,4	0,040	0,24	-	-
11	0,51	58,9	39,9	0,045	0,42	-	-
12	0,44	51,2	47,1	0,14	0,93	-	-
13	0,61	65,7	33,2	0,16	0,16	-	-
14	0,35	50,5	48,0	0,063	0,53	-	<0,56
15	0,83	69,8	28,6	0,068	0,38	-	-
16	0,25	35,9	62,8	0,094	0,76	-	-
17	0,53	63,4	35,4	0,15	0,40	-	-
18	0,76	61,3	37,2	-	0,54	-	-
19	0,53	61,4	37,1	0,12	0,56	-	-
20	0,46	60,7	37,9	0,080	0,65	-	-
21	0,17	66,9	31,6	0,44	0,71	-	-
22	0,17	57,4	41,3	0,25	0,63	-	-
23	0,16	61,0	37,9	0,24	0,50	-	-
24	0,12	49,9	49,5	0,040	0,26	-	-
25	1,15	68,0	30,1	0,099	0,40	-	-
26	0,93	66,9	31,4	0,16	0,32	-	-
27	0,18	89,3	8,05	-	0,86	0,47	<1,11

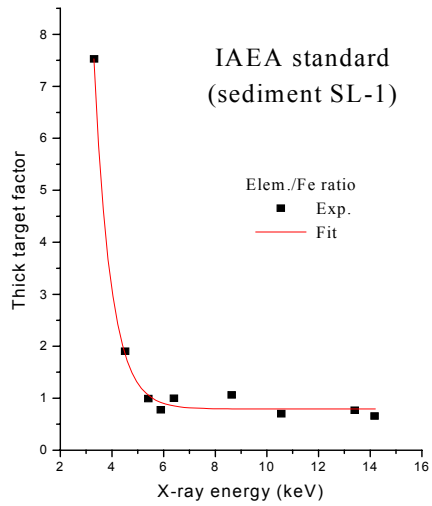


Figure 7. The thick target correction factor for the concentration ratio element / Fe in dependence of the X-ray energy, determined from the IAEA standard SL-1. The points are the experimental data and the line – a fit with an exponential function.

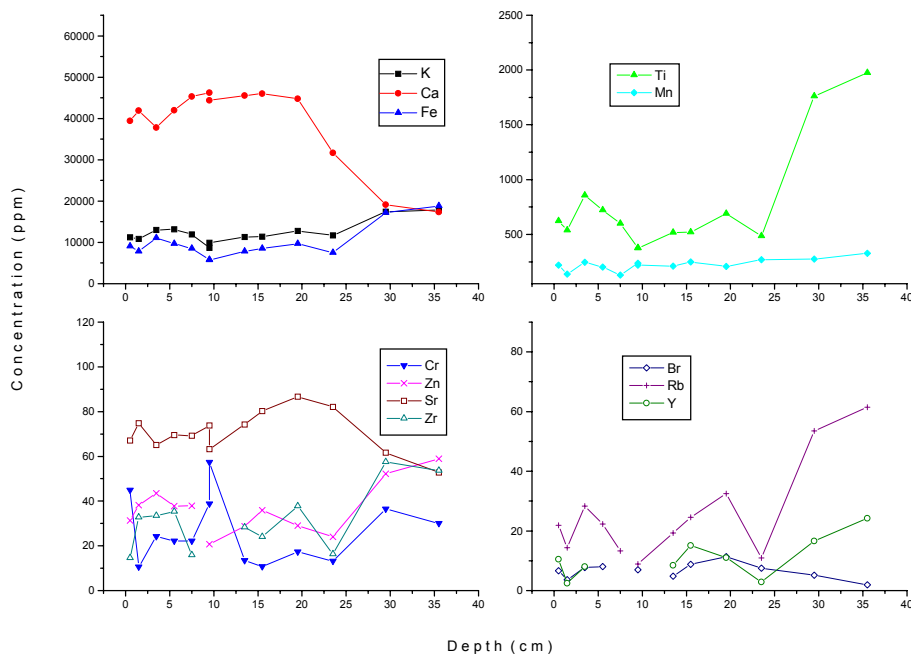


Figure 8. Concentration values (in ppm) obtained for a sediment core collected in the lake Nebunu in Danube Delta in dependence of the depth. The symbols are explained in the figure.

References

- [1] J.L. Campbell and J.A. Cockson, Nucl. Instr. and Meth. **B3**, 185 (1984).
- [2] K.G.Bauer et al., Nucl. Instr. and Meth. **148**, 407 (1978).
- [3] H. Mommsen et al., Nucl. Instr. and Meth. **166**, 361 (1979).
- [4] Z. Smit et al., Nucl. Instr. and Meth. **228**, 482 (1985).
- [5] L.-E. Carlsson and K.R. Akselsson, Nucl. Instr. and Meth. **181**, 531 (1981).
- [6] I.S. Gradshteyn and I.M. Ryzhik, *Table of integrals, series, and products* (Academic Press, Orlando, 1980).
- [7] H.H. Andersen and J.F. Ziegler, *Hydrogen stopping powers and ranges in all elements* (Pergamon Press, New York, 1977).
- [8] Vm.J. Veigele, At. Data Tables **5**, 51 (1973).
- [9] D.D. Cohen and M. Harrigan, At. Data Nucl. Data Tables **33**, 255 (1985).
- [10] M.O. Krause, J. Phys. Chem. Ref. Data **8**, 307 (1979).
- [11] S.I. Salem et al., At. Data Nucl. Data Tables **14**, 91 (1974).